Expanded beamforming models for high dynamic range scenarios

Siegfried Schlunk
Department of Biomedical Engineering
Vanderbilt University
Nashville, TN, USA
siegfried.g.schlunk@vanderbilt.edu

Brett Byram
Department of Biomedical Engineering
Vanderbilt University
Nashville, TN, USA

***Abstract*—Delay-and-sum (DAS) and many other beamformers struggle with accurately sizing targets in an ultrasound image. We previously showed that aperture domain model image reconstruction (ADMIRE) and its iterative variant (iADMIRE) can improve image quality by reducing reverberation and off-axis clutter, but they do not substantially improve upon resolution compared to DAS. Therefore, we introduce an expanded model design for the ADMIRE framework that allows for improved resolution by reducing sidelobes and show that this improved model allows iADMIRE to reach similar or better performance in terms of lateral resolution compared to minimum variance (MV). We show that this improved sidelobe performance results in improved sizing accuracy of simulated cysts compared to DAS and normal ADMIRE and iADMIRE.**

***Index Terms*—ADMIRE, iterative, dynamic range, model, beamforming, resolution**

I. INTRODUCTION

We previously introduced iterative aperture domain model image reconstruction (iADMIRE) [1], [2], an extension of ADMIRE [3]–[5] that aims to improve measured contrast accuracy in high dynamic range situations. It specifically was designed to improve performance in the presence of strong off-axis clutter that often resulted in a dark region artifact [6]. However, we noticed that while iADMIRE was able to greatly reduce off-axis clutter that originated far from the region of interest (ROI), it struggled to do so when the clutter was physically nearby. This meant that iADMIRE was unable to improve upon the resolution of delay-and-sum (DAS). This is a problem because DAS is known to under and overestimate the size of hypoechoic and hyperechoic cysts, respectively. For example, ultrasound is known to overestimate kidney stones by as much as 2-3mm [7]–[13], and stone size can determine whether invasive intervention is necessary.

In this work we introduce an expanded model for ADMIRE and iADMIRE that is designed to better handle these difficult off-axis signals, allowing for reduced sidelobes leading to improved resolution and sizing ability. We compare this new model to standard ADMIRE and iADMIRE as well as minimum variance (MV), which is well-known for its performance in enhancing lateral resolution.

II. BEAMFORMING ALGORITHMS

A. Delay-and-Sum (DAS)

Delay-and-sum (DAS) is the gold standard beamformer in part due to its low computational complexity and real-time performance. By applying a weighting factor to each channel and summing across the delayed data in those channels, each beam becomes a single line in the image. For simplicity we use rectangular apodization in this work.

B. Minimum Variance (MV)

Minimum variance (MV) is an adaptively weighted DAS image where the weighting factor is optimized to improve lateral resolution by reducing off-axis clutter [14], [15]. To ensure the covariance matrix is invertible we use recommended subarray averaging and diagonal loading methods [15]. The rest of the details are not reproduced here for space.

C. Aperture Domain Model Image Reconstruction (ADMIRE)

Aperture domain model image reconstruction (ADMIRE) is a method for removing reverberation and off-axis clutter, and suppressing wavefront aberration. Byram et al. presented a detailed explanation of the components of the algorithm [4], and additional information can be found elsewhere [3], [5].

Processing begins by dividing delayed channel data into multiple overlapping windows along the axial dimension, along which the Fourier transform is performed (i.e. a short-time Fourier transform (STFT)). This data can then be analyzed for each primary frequency component using a physics-based model derived from the well-defined physics of linear wave propagation. It is composed of the predicted aperture domain signals created from scatterers throughout the field-of-view of the transducer, which are combined into a model matrix, X, each signal corresponding to some physical location in the imaging space. This allows us to represent a given domain signal, y, by its component sources, β, by

$$y = X\beta, \tag{1}$$

where y is for a specific wave number k and location (x_n, z_n), X is the set of physical model predictors, and β the set of solved model coefficients. Due to the ill-posed nature

978-1-7281-5448-0/20/$31.00 ©2020 IEEE

of the problem, ADMIRE uses the elastic-net regularization technique [16] with the optimization equation

$$\hat{\beta} = \arg\min_{\beta}(||y - X\beta||^2 + \lambda(\alpha||\beta||_1 + (1-\alpha)||\beta||_2^2/2)), \tag{2}$$

where $||\beta||_1$ is the L1 norm, $||\beta||_2$ is the L2 norm, and α is set between 0 and 1 to control the weighting between L1 and L2. λ is a regularization parameter which controls the degrees of freedom [17]. Here, we choose $\alpha = 0.9$ and $\lambda_{\text{LDF}} = (0.0189/10)y_{\text{RMS}}$ based on the root mean square (RMS) of the signal y.

Solving 2 gives us an estimate of β, which reveals the specific physical locations of the various reflected echoes that linearly combine to form y. For the current location being processed, ADMIRE then chooses some small region of interest (ROI) centered at that location and can simply remove the coefficients for sources outside of that ROI, and reconstruct the decluttered signal as

$$y_{\text{decluttered}} = X\beta_{\text{ROI}}, \tag{3}$$

using only the coefficients β_{ROI} corresponding to signals originating from inside the ROI. This removes any signals located off-axis or from reverberant sources.

Once the aperture domain signal has been decluttered using the coefficients solved by the elastic-net and (3), the inverse STFT is applied to return to the time domain [18]. This results in a decluttered version of the channel data that can still be processed using other beamformers.

D. *Iterative ADMIRE (iADMIRE)*

Iterative ADMIRE (iADMIRE) is a modification to the ADMIRE algorithm that seeks to accommodate environments with high dynamic ranges by mitigating the shortcomings of the elastic-net [1], [2]. Specifically, the L1 characteristics of the elastic-net can result in weak signals being zeroed out in favor of stronger sources, which can result in a dark region artifact where only the strong clutter coefficients are fit, zeroing everything from the region of interest.

Algorithm 1 shows the process by which iADMIRE iteratively solves for the clutter sources in the signal and removes them, theoretically obtaining a more accurate estimate of the ROI signal. Rather than doing a single solve for the model coefficients and reconstructing only the ROI signal, iADMIRE computes the clutter-only signal y_{clutter} using (4) and the coefficients β_{clutter} corresponding to the clutter predictors in the model and subtracts that from the original signal with (5). By iteratively applying the elastic-net and removing the reconstructed clutter signal from the signal, strong clutter sources are continually removed until some threshold is reached. This new, less cluttered signal is then decomposed using the elastic-net one last time to produce the decluttered signal using (3).

Algorithm 1: Iterative clutter removal in ADMIRE

```
Given model predictors $X = [X_{\text{ROI}}\ X_{\text{clutter}}]$, aperture
  domain signal $y_1$, parameters $\alpha$ and $\lambda$, and $\delta > 0$
for $i = 1$ do
    Solve (2) for model coefficients $\hat{\beta}_i$, given $y_i$, $X$
    Compute clutter-only signal
        $y_{i,\text{clutter}} = X_{\text{clutter}}\hat{\beta}_{i,\text{clutter}}$    (4)
    Compute new aperture signal
        $y_{i+1} = y_i - y_{i,\text{clutter}}$    (5)
    Stop when $||y_{i+1} - y_i||_2^2 < \delta$
end for
Calculate $y_{\text{decluttered}} = X_{\text{ROI}}\hat{\beta}_{i,\text{ROI}}$
```

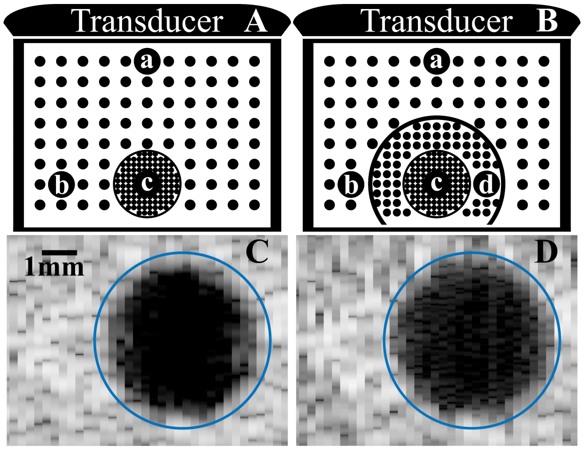

Fig. 1. (A) standard ADMIRE model space. (B) expanded model space designed to better classify difficult off-axis signals. (C) b-mode image of a 5mm simulated cyst processed with iADMIRE, showing the difference between the true cyst edges (blue) and the apparent visible edges. (D) the same 5mm cyst processed with the expanded model.

E. *Expanded ADMIRE Model*

Fig. 1C shows an example of the issue presented here. The visible edges of the simulated cyst differ significantly from the true edges of the cyst, which will result in underestimating the size. Similarly, hyperechoic cysts will be overestimated due to the failure of the elastic-net to classify these difficult off-axis signals as clutter, resulting in higher sidelobes and lower lateral resolution than ideal. In the case of ADMIRE, the mechanism at fault is a preference of the elastic-net to classify signals as ROI signals due to the high sampling in that model space, but this crossover only occurs if the signals are sufficiently similar, i.e. physically located nearby.

The proposed solution is to make a modification to the standard model, also shown in Fig. 1. The model in (A) shows an example of the normal ADMIRE model space, and (B) shows the expanded model. Specifically, this expanded model creates an additional region (d) that is more highly sampled than the normal clutter (a,b) while less highly sampled than the actual ROI area (c). This should allow the elastic-net to more accurately classify these off-axis signals and properly reject them. In this work, we implement two variants of the expanded model: one where the expanded model is applied everywhere (iADMIRE-EM), and one where the expanded

TABLE I
FIELD II SIMULATION PARAMETERS FOR CONTRAST TARGET PHANTOMS

Parameter	Value
Number of elements	117
Number of mathematical elements (lateral)	7
Number of mathematical elements (elevation)	11
Element height	4 mm
Element width	0.254 mm
Kerf	0.003 mm
Lateral pitch	0.257 mm
Center frequency (f_c)	3 MHz
Sampling frequency (simulation) (f_s)	640 Mhz
Sampling frequency (downsampled) (f_s)	40 MHz
Bandwidth	60%
Transmit focal depth	3 cm
Transmit/receive f-number	1

TABLE II
MEAN POINT TARGET WIDTH AT VARYING LEVELS

	Point Target Width (mm)		
Intensity (dB)	-6 (FWHM)	-10	-20
DAS	0.56±.00	0.73±.01	0.99±.02
MV	**0.23±.00**	0.31±.00	0.59±.02
ADMIRE	0.49±.02	0.68±.01	0.90±.02
iADMIRE	0.50±.01	0.68±.01	0.90±.02
iADMIRE-EM	**0.23±.00**	**0.30±.01**	**0.45±.01**
iADMIRE-sEM	0.36±.01	0.47±.01	0.57±.01

model is selectively applied in areas where the elastic-net detects these difficult off-axis signals (iADMIRE-sEM).

III. METHODS

A. Cyst Sizing Phantom

We used Field II [19], [20] to simulate n=6 5mm cysts of varying intensities (anechoic, -50 dB to 70 dB). The simulation parameters are detailed in Table I. For each phantom and each beamforming method, the cyst size was estimated and the correlation of the background speckle region directly adjacent to the cyst was measured against the true speckle (no cyst present) to determine the accuracy of the speckle. The correlation was calculated as

$$r = \frac{\sum_x \sum_z (S(x,z) - \mu_S)(D(x,z) - \mu_D)}{\sqrt{(\sum_x \sum_z (S(x,z) - \mu_S)^2)(\sum_x \sum_z (D(x,z) - \mu_D)^2)}}, \tag{6}$$

where S is the enveloped, uncompressed region of the data for the beamformer of interest, and D is short-hand for the reference DAS enveloped, uncompressed region of data. Values of r closer to 1 indicate more accurate speckle.

B. Lateral Resolution Phantom

We additionally simulated n=6 single target scatterers to measure more precisely lateral resolution by measuring the mean lateral width at varying levels: -6 dB (full width at half maximum), -10 dB, and -20 dB.

IV. RESULTS

Fig. 2 shows a sample realization of a 5mm anechoic and 60 dB cyst, where the blue line indicates the true edges of the cyst. Visibly DAS, ADMIRE, and iADMIRE all underestimate the size of the anechoic cyst while overestimating the size of the hyperechoic cyst. iADMIRE-EM and iADMIRE-sEM show relative improvement, both axially and laterally. This can be further seen in Fig. 3, which shows the average measured cyst size across the varying intensities, demonstrating that the expanded model improved sizing across all cases. Finally, we include the mean point target width in Table II. We again see that DAS, ADMIRE, and iADMIRE are all on par with each other, and the expanded model variants show a marked improvement comparatively. In fact, iADMIRE-EM performs as well or better than MV.

The rational for the inclusion of iADMIRE-sEM is seen in Fig. 4, showing that the expanded model does have a negative effect on the representation of the background speckle. Selectively applying the expanded model does result in a slight improvement to the speckle accuracy compared to using the expanded model everywhere. This produces a more balanced result, somewhere between iADMIRE and iADMIRE-EM. Both expanded model variants have improved sidelobe performance which results in improved speckle accuracy in the higher intensity cases, especially at 40 and 50 dB.

V. DISCUSSION AND CONCLUSIONS

We have shown that the expanded ADMIRE model is able to improve resolution and sizing accuracy by reducing sidelobes, attaining performance on par with MV in terms of lateral resolution. When resolution or sizing is most important, the iADMIRE-EM method demonstrates consistently better performance compared to DAS and the normal ADMIRE model. The selective iADMIRE-sEM method did somewhat mitigate the loss of the background speckle accuracy, though in its current state we would most likely choose to either just use the expanded or normal model, depending on what aspect of an image is being prioritized.

ACKNOWLEDGMENT

The authors would like to thank the staff of the Vanderbilt University ACCRE computing resource. This work was supported by NIH grants R01EB020040 and S10OD016216-01, and additionally by NSF award IIS-1750994.

REFERENCES

[1] S. Schlunk, K. Dei, and B. Byram, "Iterative ADMIRE for High Dynamic Range B-Mode," *IEEE International Ultrasonics Symposium (IUS)*, vol. 2018-Octob, pp. 1–4, 2018.

[2] ——, "Iterative model-based beamforming for high dynamic range applications," *IEEE Transactions on Ultrasonics, Ferroelectrics, and Frequency Control*, pp. 1–1, 2020.

[3] B. Byram and M. Jakovljevic, "Ultrasonic Multipath and Beamforming Clutter Reduction: A Chirp Model Approach," *IEEE Transactions on Ultrasonics, Ferroelectrics, and Frequency Control*, vol. 61, no. 3, pp. 428–440, 2014.

[4] B. Byram, K. Dei, J. Tierney, and D. Dumont, "A Model and Regularization Scheme for Ultrasonic Beamforming Clutter Reduction," *IEEE Transactions on Ultrasonics, Ferroelectrics, and Frequency Control*, vol. 62, no. 11, pp. 1913–1927, 2015.

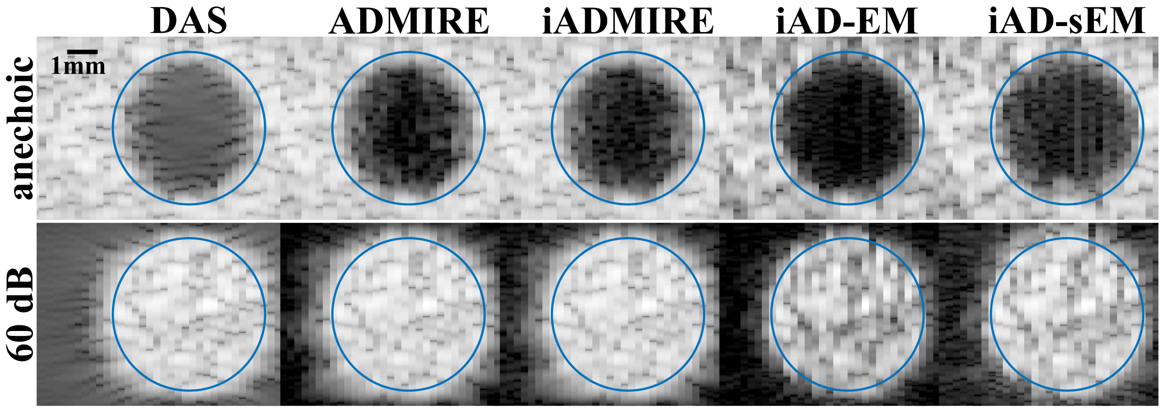

Fig. 2. B-mode images on an 80 dB dynamic range for an example anechoic and 60 dB cyst processed with each method.

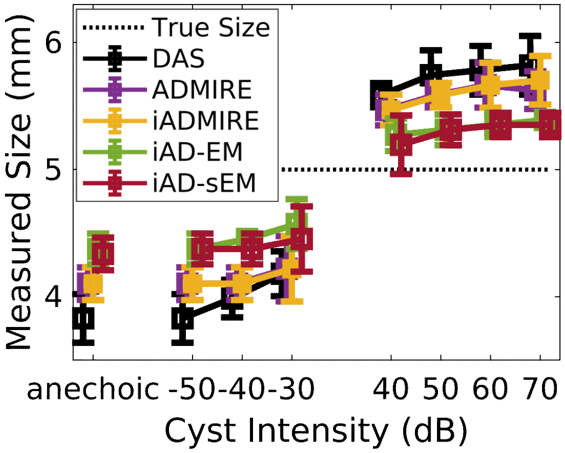

Fig. 3. Measured cyst size for each method across the various intensity cysts compared to the true size (5mm). Error bars indicate standard deviation.

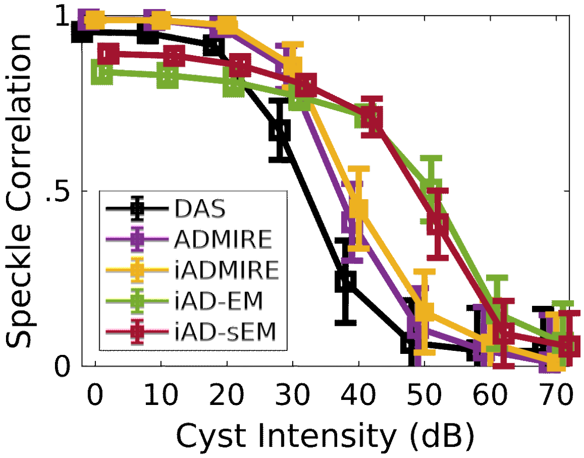

Fig. 4. Speckle correlation directly adjacent to the cyst (location of difficult off-axis clutter). Values closer to 1 indicate more accurate speckle.

[5] K. Dei and B. Byram, "The Impact of Model-Based Clutter Suppression on Cluttered, Aberrated Wavefronts," *IEEE Transactions on Ultrasonics, Ferroelectrics, and Frequency Control*, vol. 64, no. 10, pp. 1450–1464, 2017.

[6] O. M. H. Rindal, A. Rodriguez-Molares, and A. Austeng, "The Dark Region Artifact in Adaptive Ultrasound Beamforming," *IEEE International Ultrasonics Symposium (IUS)*, pp. 1–4, 2017.

[7] S. Ulusan, Z. Koc, and N. Tokmak, "Accuracy of sonography for detecting renal stone: Comparison with CT," *Journal of Clinical Ultrasound*, vol. 35, no. 5, pp. 256–261, 6 2007. [Online]. Available: http://doi.wiley.com/10.1002/jcu.20347

[8] D. Unal, E. Yeni, M. Karaoglanoglu, A. Verit, and O. F. Karatas, "Can Conventional Examinations Contribute to the Diagnostic Power of Unenhanced Helical Computed Tomography in Urolithiasis?" *Urologia Internationalis*, vol. 70, no. 1, pp. 31–35, 2003. [Online]. Available: https://www.karger.com/Article/FullText/67702

[9] A. A. Ray, D. Ghiculete, K. T. Pace, and R. J. D. Honey, "Limitations to Ultrasound in the Detection and Measurement of Urinary Tract Calculi," *Urology*, vol. 76, no. 2, pp. 295–300, 8 2010. [Online]. Available: https://linkinghub.elsevier.com/retrieve/pii/S0090429509030799

[10] V. Ganesan, S. De, D. Greene, F. C. M. Torricelli, and M. Monga, "Accuracy of ultrasonography for renal stone detection and size determination: is it good enough for management decisions?" *BJU International*, vol. 119, no. 3, pp. 464–469, 3 2017. [Online]. Available: http://doi.wiley.com/10.1111/bju.13605

[11] K. A. B. Fowler, J. A. Locken, J. H. Duchesne, and M. R. Williamson, "US for Detecting Renal Calculi with Nonenhanced CT as a Reference Standard," *Radiology*, vol. 222, no. 1, pp. 109–113, 1 2002. [Online]. Available: http://pubs.rsna.org/doi/10.1148/radiol.2221010453

[12] B. Dunmire, F. C. Lee, R. S. Hsi, B. W. Cunitz, M. Paun, M. R. Bailey, M. D. Sorensen, and J. D. Harper, "Tools to Improve the Accuracy of Kidney Stone Sizing with Ultrasound," *Journal of Endourology*, vol. 29, no. 2, pp. 147–152, 2 2015. [Online]. Available: http://www.liebertpub.com/doi/10.1089/end.2014.0332

[13] K. M. Sternberg, B. Eisner, T. Larson, N. Hernandez, J. Han, and V. M. Pais, "Ultrasonography Significantly Overestimates Stone Size When Compared to Low-dose, Noncontrast Computed Tomography," *Urology*, vol. 95, pp. 67–71, 9 2016. [Online]. Available: https://linkinghub.elsevier.com/retrieve/pii/S0090429516302710

[14] I. K. Holfort, F. Gran, and J. A. Jensen, "Broadband minimum variance beamforming for ultrasound imaging," *IEEE Transactions on Ultrasonics, Ferroelectrics, and Frequency Control*, vol. 56, no. 2, pp. 314–325, 2009.

[15] J.-F. Synnevåg, A. Austeng, and S. Holm, "Adaptive Beamforming Applied to Medical Ultrasound Imaging," *IEEE Transactions on Ultrasonics, Ferroelectrics, and Frequency Control*, vol. 54, no. 8, pp. 1606–1613, 2007.

[16] H. Zou and T. Hastie, "Regularization and variable selection via the elastic net," *Journal of the Royal Statistical Society: Series B (Statistical Methodology)*, vol. 67, no. 2, pp. 301–320, 2005.

[17] R. J. Tibshirani and J. Taylor, "Degrees of Freedom in Lasso Problems," *The Annals of Statistics*, vol. 40, no. 2, pp. 1198–1232, 2012.

[18] B. Yang, "A Study of Inverse Short-Time Fourier Transform," *IEEE International Conference on Acoustics, Speech and Signal Processing*, pp. 3541–3544, 2008.

[19] J. A. Jensen, "Field: A Program for Simulating Ultrasound Systems," *Paper presented at the 10th Nordic-Baltic Conference on Biomedical Imaging Published in Medical & Biological Engineering and Computing*, vol. 34, pp. 351–353, 1996.

[20] J. A. Jensen and N. B. Svendsen, "Calculation of Pressure Fields from Arbitrarily Shaped, Apodized, and Excited Ultrasound Transducers," *IEEE Transactions on Ultrasonics, Ferroelectrics, and Frequency Control*, vol. 39, pp. 262–267, 1992.